Supporting Information

Enhancing the J_{SC} of P3HT-Based OSCs via a Thiophene-Fused Aromatic Heterocycle as a "π-Bridge" for A-π-D-π-A Type Acceptors

Jiacheng Wang,[†] Tengfei Li,[‡] Xiaoxiao Wang,[†] Yiqun Xiao,[§] Cheng Zhong,[†] Jiayu Wang,[‡] Kuan Liu,[‡] Xinhui Lu,[§] Xiaowei Zhan,*[,‡] and Xingguo Chen*[,†]

[†] Hubei Key Laboratory on Organic and Polymeric Opto-electronic Materials, College of Chemistry and Molecular Sciences, Wuhan University, Wuhan 430072, China

[‡] Department of Materials Science and Engineering, College of Engineering, Peking University, Beijing 100871, China

[§] Department of Physics, Chinese University of Hong Kong, New Territories 999077, Hong Kong, China

Corresponding Authors

*E-mail: xgchen@whu.edu.cn (X.C.)

*E-mail: xwzhan@pku.edu.cn (X.Z.)

Instruments and measurements

^{1}H-NMR and ^{13}C-NMR were measured on a Bruker AVANCE III HD 400MHz. ESI-MS analysis was determined on a Finnigan-LCQ advantage mass spectrometer. MALDI-TOF analysis was performed on an Applied Biosystems 4700 proteomics Analyzer 155 mass spectrometer. The thermogravimetric analysis (TGA) was performed on TA thermal analyzer (model Q600 SDT) under a nitrogen flow at a heating rate of 10 ^{o}C min^{-1}. The thickness of active layer was measured on a Bruker DektakXT profilometer. Elemental analyses were carried out on a 73 CARLOERBA-1106 microelemental analyzer. The electronic energy levels were measured by electrochemical cyclic voltammetry (CV) and refer to the Leeuw empirical formula: HOMO = -(E_{onset}^{ox} + 4.8 − 0.48); LUMO = -(E_{onset}^{red} + 4.8 − 0.48). The CV was conducted on a CHI voltammetric analyzer with glassy carbon disk, Pt wire and Ag/Ag^{+} electrode as working electrode, counter electrode and reference electrode respectively in a 0.1 mol L^{-1} tetrabutylammonium hexafluorophosphate (Bu$_4$NPF$_6$) acetonitrile solution. The UV-vis absorption spectra of the materials were measured by a Varian Cary 5000 UV-vis-NIR spectrophotometer. Atomic force microscope (AFM) images were measured on Multimode 8 scanning probe microscopy (Bruker Daltonics Inc., United States) in the tapping mode in order to investigate the nanoscale morphology of the blends. The transmission electron microscopy (TEM) characterization was carried out on a JEM-2100 transmission electron microscope operated at 200 kV. Density functional theory (DFT) calculations were employed at B3LYP/def2-SVP level and the dispersion correction was conducted by Grimme's D3 version with BJ damping function. The electronic structures were obtained at same level of theory and all calculations were done with Gaussian09 software. The GIWAXS/GISAXS measurements are conducted at 14B1 and 19U2 beamline at Shanghai Synchrotron Radiation Facility, Shanghai, China with 10 keV primary beam,

0.15° incidence angle and Mar 225 CCD and Pilatus 1M-F detector, respectively. The samples for GIWAXS measurements are fabricated on silicon substrates using the same recipe for the devices.

Fabrication and characterization of organic solar cells

Organic solar cells were fabricated with the structure: ITO/ZnO/active layer/MoO$_3$/Ag. The indium tin oxide (ITO) glass (sheet resistance = 10 Ω sq^{-1}) was pre-cleaned in an ultrasonic bath of deionized water, acetone and isopropanol. ZnO layer (*ca.*30 nm) was spin-coated onto the ITO glass from ZnO precursor solution (100 mg Zn(CH$_3$COO)$_2$·2H$_2$O and 0.02 mL ethanolamine dissolved in 1 mL 2-methoxyethanol), and baked at 200 °C for 30 min. A chloroform solution of P3HT:acceptor (15 mg mL^{-1} in total) was spin-coated on ZnO layer to form a photoactive layer. The MoO$_3$ layer (*ca.*5 nm) and Ag (100 nm for opaque devices) were successively evaporated onto the surface of the photoactive layer under vacuum (*ca.*10^{-5}Pa). The active area of the device was 4.0 mm^2, defined under an optical microscope. The *J-V* curve was measured using a computer-controlled B2912A Precision Source/Measure Unit (Agilent Technologies). An XES-70S1 (SAN-EI Electric Co., Ltd.) solar simulator (AAA grade, 70 × 70 mm^{2}photobeam size) coupled with AM 1.5G solar spectrum filters was used as the light source, and the optical power at the sample was 100 mW cm^{-2}. A 2 × 2 cm^2 monocrystalline silicon reference cell (SRC-1000-TC-QZ) was purchased from VLSI Standards Inc. The EQE spectra were measured using a Solar Cell Spectral Response Measurement System QE-R3011 (Enlitech Co., Ltd.). The light intensity at each wavelength was calibrated using a standard single crystal Si photovoltaic cell.

Mobility measurements

Hole-only and electron-only diodes were fabricated using the architectures: ITO/PEDOT:PSS/P3HT:acceptor/Au for holes and ITO/ZnO/P3HT:acceptor/Al or ITO/ZnO/acceptor/Al for electrons. Mobilities were extracted by fitting the current density–voltage curves using space-charge-limited current (SCLC) method. The J-V curves of the devices were plotted as $\ln(Jd^3/V^2)$ versus $(V/d)^{0.5}$ using the equation $\ln(Jd^3/V^2) \cong 0.89(1/E0)^{0.5}(V/d)^{0.5} + \ln(9\varepsilon_0\varepsilon_r\mu/8)$, where J is the current density, d is the film thickness of active layer, μ is the hole or electron mobility, ε_r is the relative dielectric constant of the transport medium, ε_0 is the permittivity of free space ($8.85 \times 10^{-12}\,\text{F m}^{-1}$), $V = V_{appl} - V_{bi}$, where V_{appl} is the applied voltage to the device, and V_{bi} is the built-in voltage due to the difference in work function of the two electrodes (for hole-only diodes, V_{bi} is 0.2 V; for electron-only diodes, V_{bi} is 0 V).

Table S1. The parameters of P3HT:JC2 or JC1 based devices with optimized D/A ratios and different solvent additive.

Devices	Additive (v/v)	V_{OC} (V)	J_{SC} (mA/cm^2)	FF (%)	PCE (%)
	w/o	0.88	1.25	30.0	0.33
	0.5% DIO	0.71	13.41	51.9	4.93
P3HT:JC2[a]	1% DIO	0.70	12.85	59.2	5.29
	1.5% DIO	0.69	12.56	56.5	4.90
	0.5% CN	0.74	9.65	47.6	3.41
	w/o	0.67	0.45	29.6	0.09
P3HT:JC1[b]	0.5% DIO	0.47	4.09	40.1	0.78
	0.5% CN	0.51	4.00	42.8	0.87

[a]D/A radio of 1:0.8; [b]D/A radio of 1:0.6.

Table S2. The parameters of P3HT:JC2 or JC1 based devices with annealing conditions at 140 °C/10 min and different D/A ratios.

Devices	D:A (w/w)	V_{OC} (V)	J_{SC} (mA/cm^2)	FF (%)	PCE (%)
P3HT:JC2	1:1	0.70	14.06	53.5	5.26
	1:0.8	0.71	13.82	60.8	5.95
	1:0.6	0.71	9.55	64.2	4.34
P3HT:JC1	1:0.8	0.46	8.76	53.6	2.17
	1:0.6	0.48	10.54	55.8	2.80
	1:0.4	0.49	7.96	53.3	2.07

Table S3. The parameters of P3HT:JC2 or JC1 based devices with different annealing temperature for 10 min.

Devices	Temperature (°C)	V_{OC} (V)	J_{SC} (mA/cm^2)	FF (%)	PCE (%)
P3HT:JC2[a]	130	0.71	13.73	55.6	5.44
	140	0.71	13.04	64.4	5.99
	150	0.71	13.1	61.7	5.70
P3HT:JC1[b]	130	0.47	9.31	45.2	1.99
	140	0.48	10.54	55.8	2.80
	150	0.48	10.22	52.3	2.55

[a]D/A radio of 1:0.8; [b]D/A radio of 1:0.6.

Table S4. The parameters of P3HT:JC2 based devices with D/A radio of 1:0.8 and different annealing time at 140 °C.

Device	Time (min)	V_{OC} (V)	J_{SC} (mA/cm^2)	FF (%)	PCE (%)
P3HT:JC2	5	0.71	12.89	59.0	5.38
	10	0.71	13.96	62.6	6.24
	15	0.71	13.86	57.4	5.62
	20	0.71	13.47	59.2	5.67

Table S5. Carrier transport properties of acceptor neat films and optimized P3HT:acceptor blended films.

Acceptor	$\mu_e{}^a$ (cm^2 V^{-1} s^{-1})	$\mu_h{}^b$ (cm^2 V^{-1} s^{-1})	$\mu_e{}^b$ (cm^2 V^{-1} s^{-1})	μ_h/μ_e
JC2	4.10×10^{-4}	5.02×10^{-5}	4.54×10^{-5}	1.11
JC1	5.00×10^{-4}	5.55×10^{-5}	1.51×10^{-4}	0.37

[a]Acceptor neat films; [b]optimized P3HT:JC2 or P3HT:JC1 blended films.
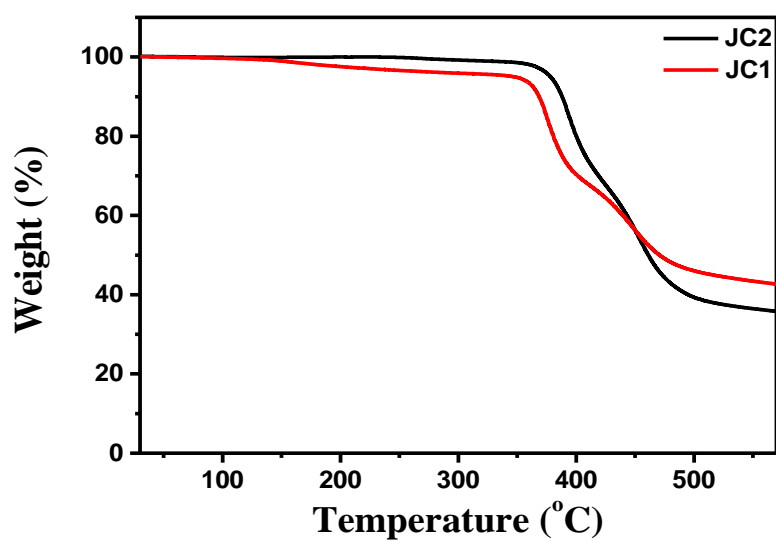
Figure S1. The TGA curves of JC1 and JC2.
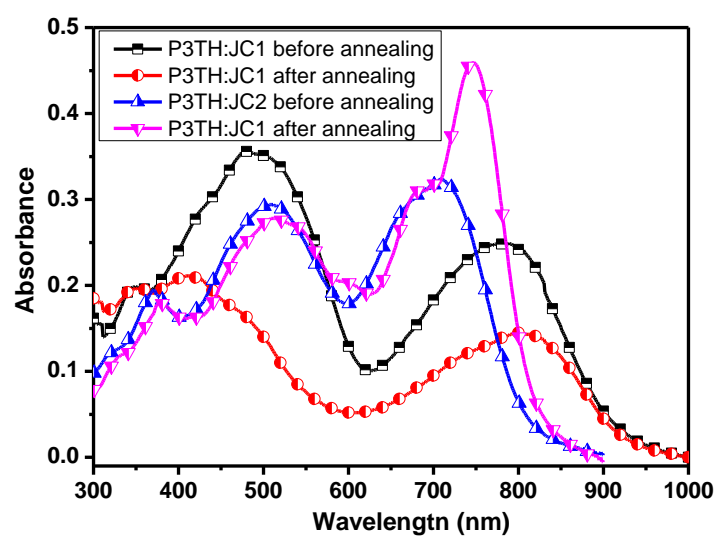
Figure S2. The absorption of P3TH:JC1 and P3TH:JC2 blended films before and after annealing.
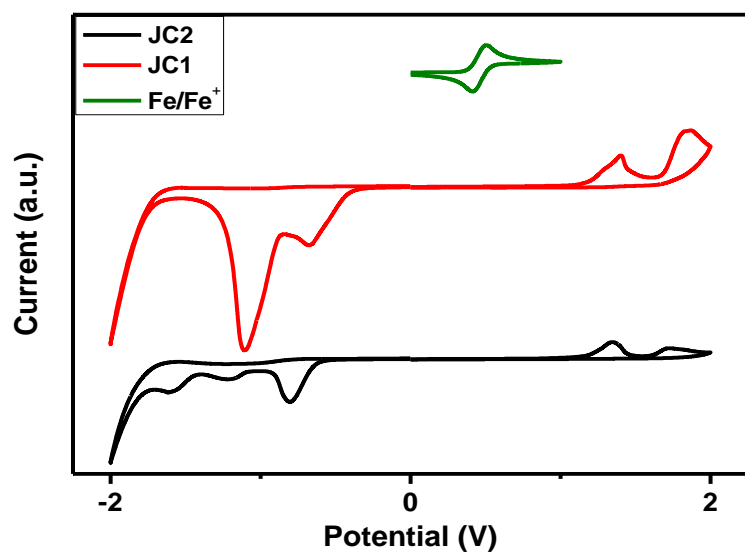
Figure S3. The CV curves of JC1 and JC2 in CH_3CN/0.1 M Bu_4NPF_6 at 100 mV s^{-1}.
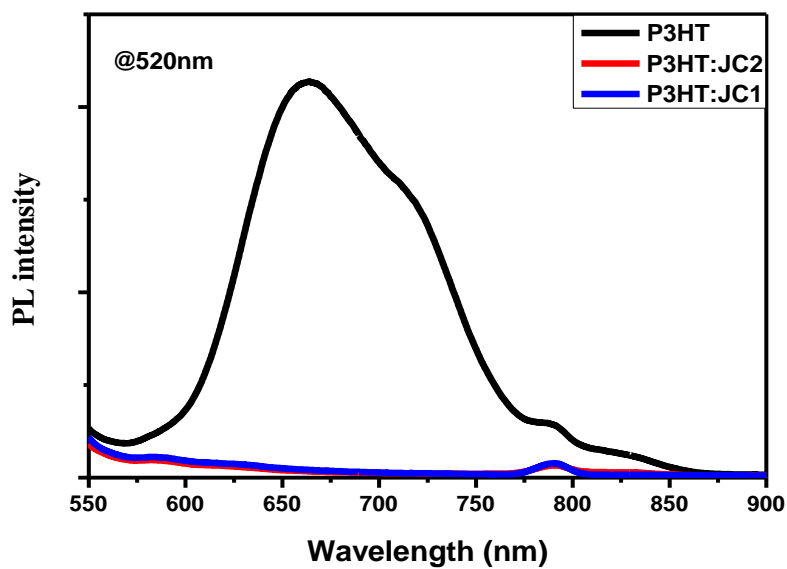
Figure S4. Photoluminescence spectra of the P3HT film, optimized P3HT:JC1 blended film and P3HT:JC2 blended film excited at 520 nm.
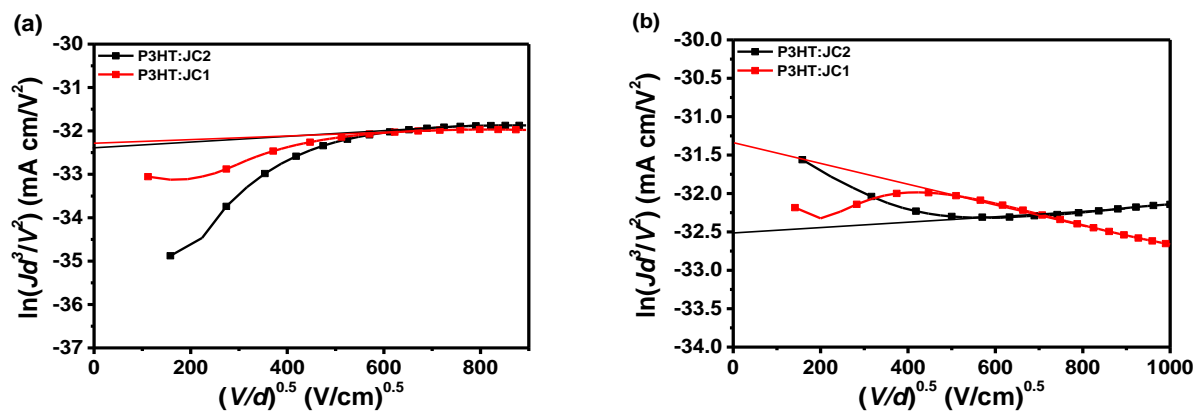
Figure S5. Ln(JL^3/V^2) vs (V/L)$^{0.5}$ plot for the hole mobility (a) and electron mobility (b)

measurements based on optimized P3HT:JC1 and P3HT:JC2 blended films.
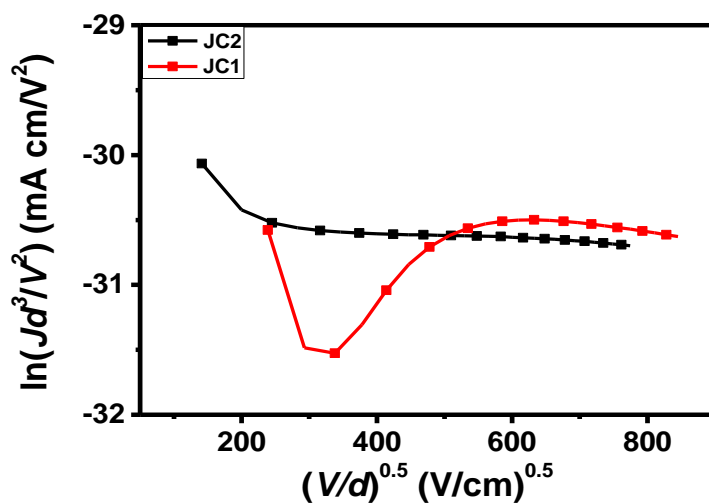
Figure S6. Ln(JL^3/V^2) vs (V/L)$^{0.5}$ plot for the electron mobility measurement based on neat JC1 and

JC2 films.
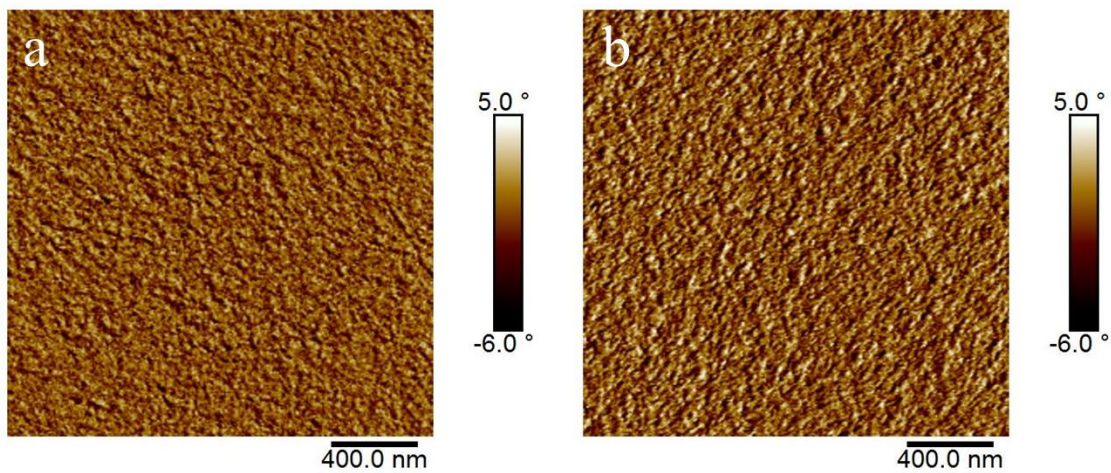
Figure S7. AFM phase images of (a) optimized P3HT:JC2 and (b) optimized P3HT:JC1 blended films.
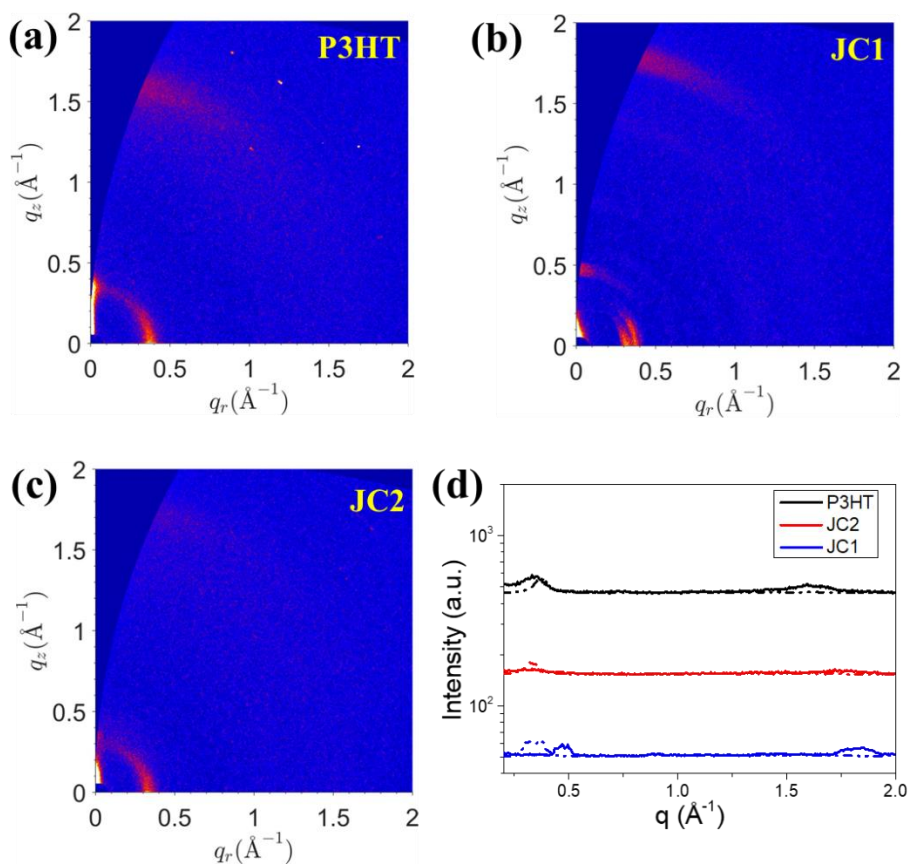
Figure S8. 2D GIWAXS patterns of pure (a) P3HT, (b) JC1 and (c) JC2; (d) the corresponding intensity profiles along the in-plane (dashed line) and out-of-plane (solid line) directions.
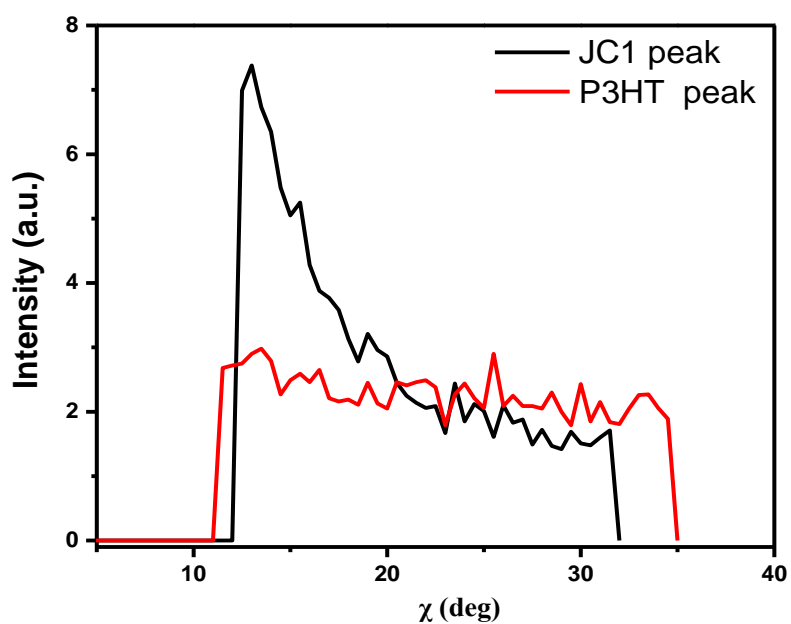
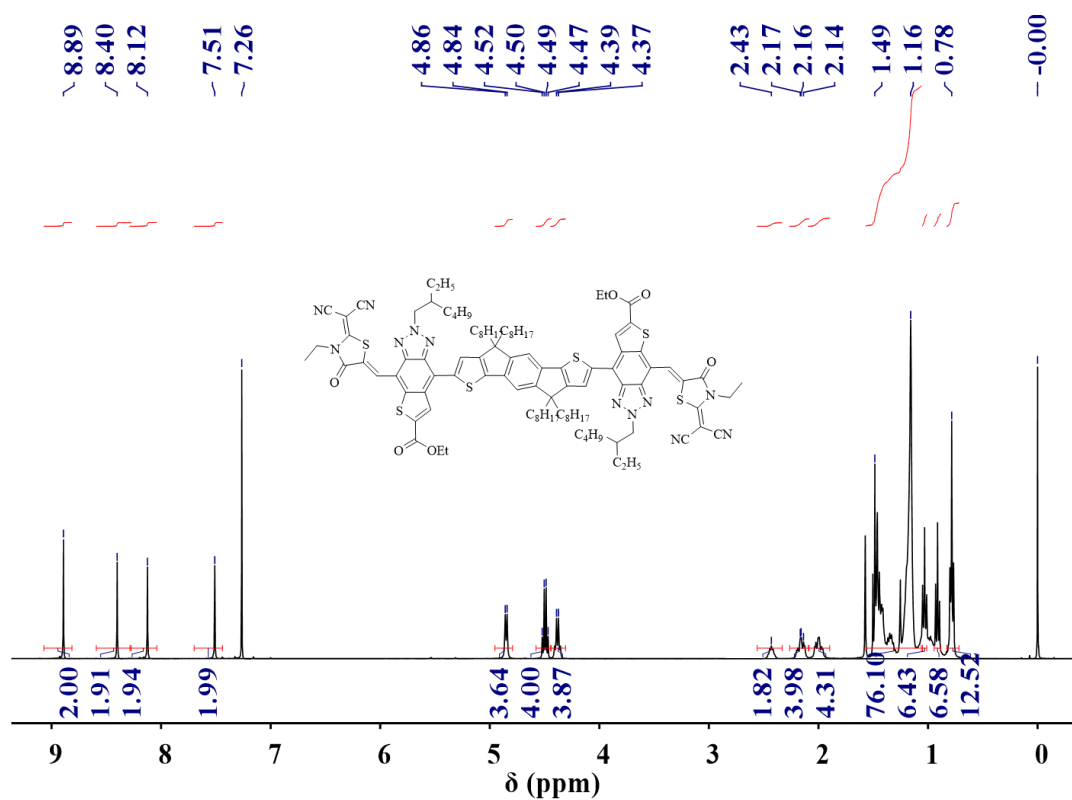**Figure S9**. π-π peak of JC1 (black) and P3HT (red) along ring profiles of optimized P3HT:JC1 blended film.
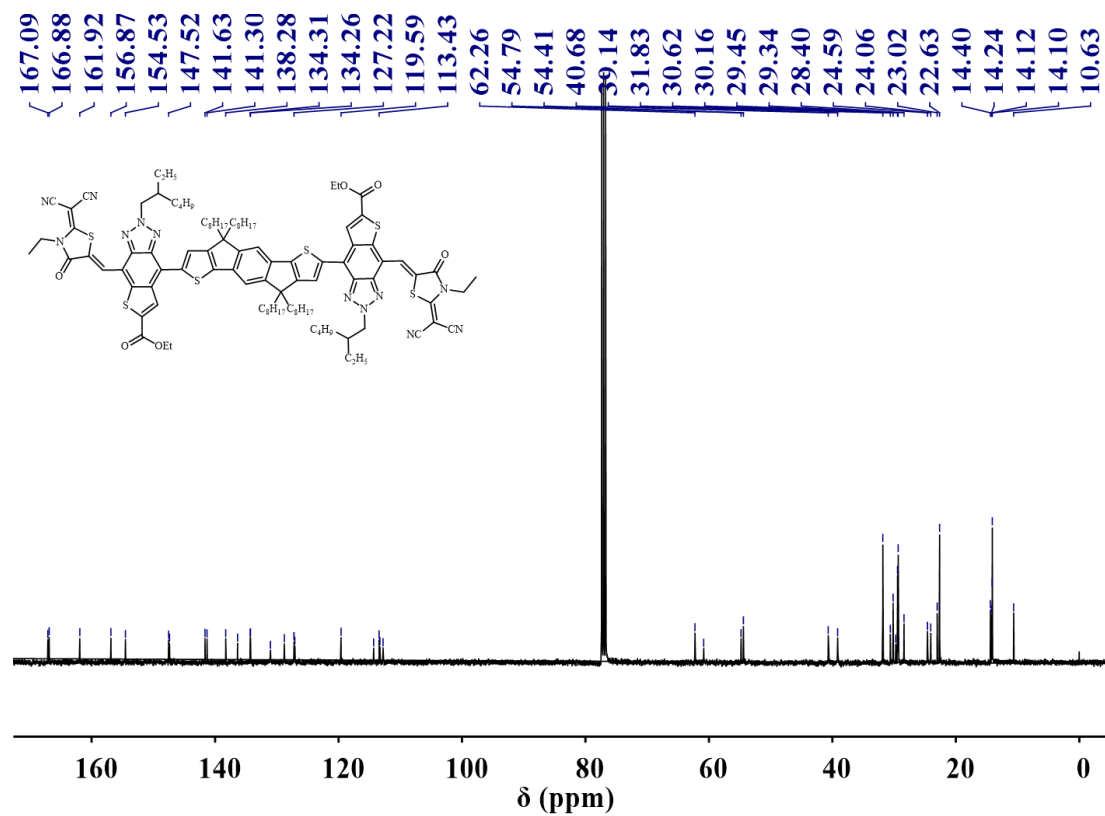

Figure S10 ^{1}H NMR spectrum of JC2.
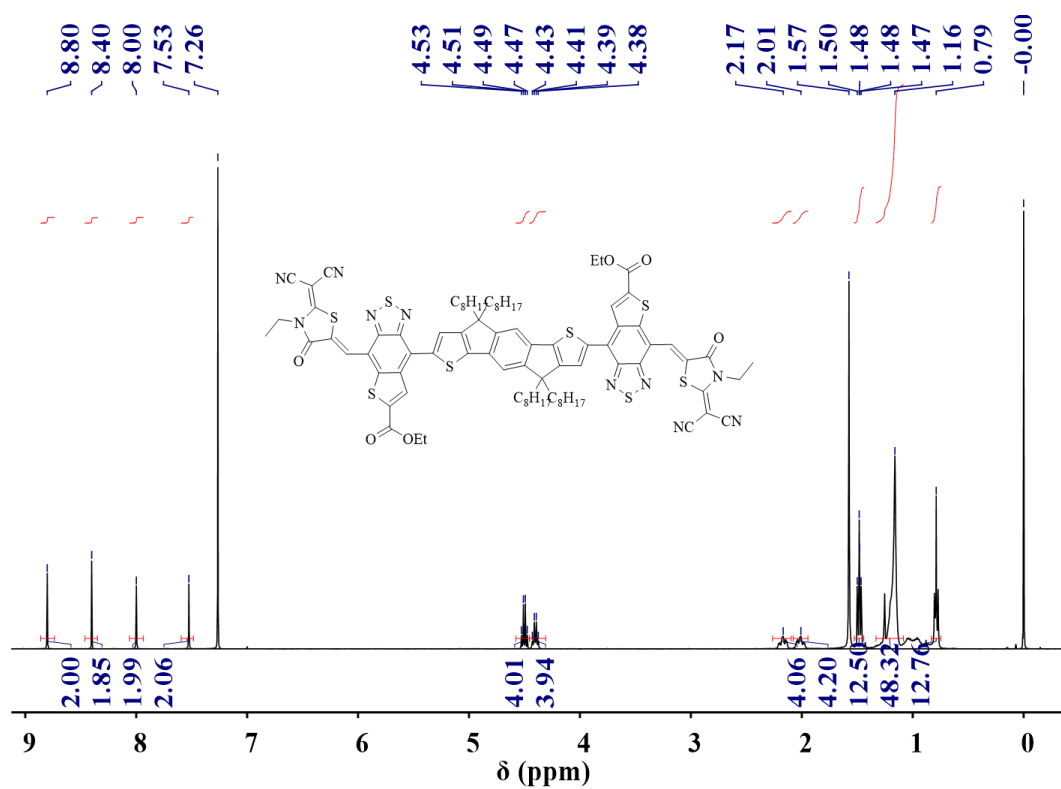
Figure S11. ^{13}C NMR spectrum of JC2.

Figure S12. ^{1}H NMR spectrum of JC1.
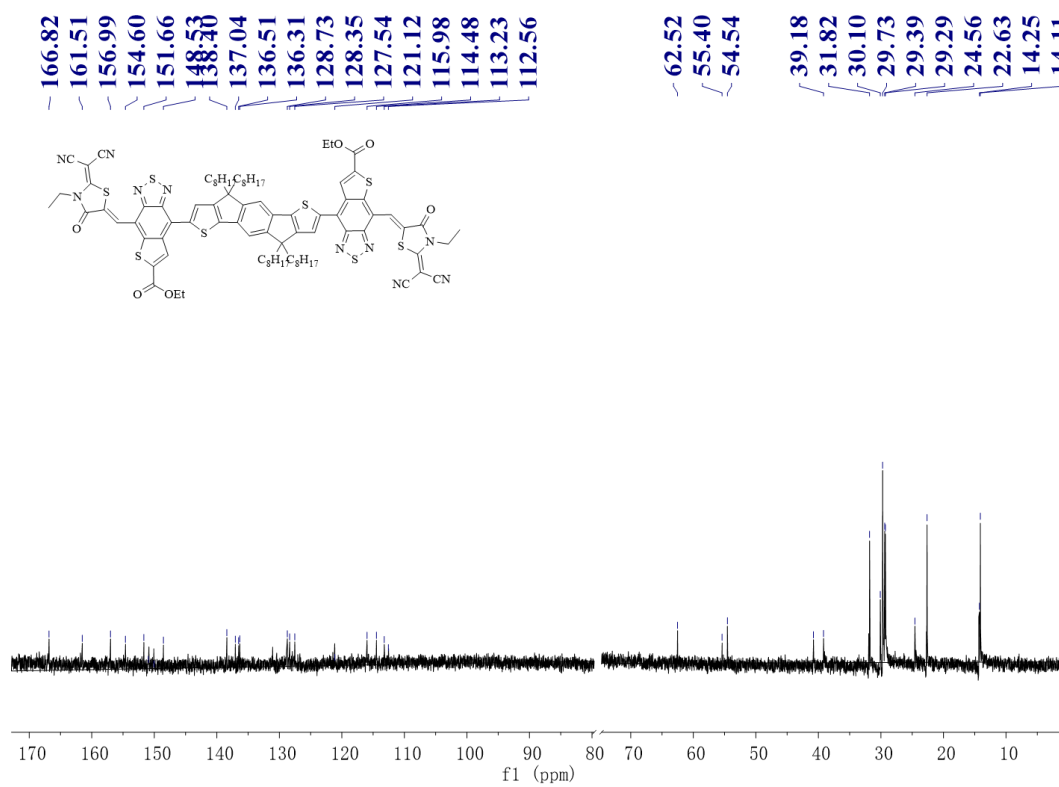
Figure S13. ^{13}C NMR spectrum of JC1.